VIII International Conference on Particle-Based Methods
PARTICLES 2023
U. Perego, M. Cremonesi, A. Franci (Eds)

EXAMINATION OF THE INFLUENCE OF PARTICLE PARAMETERS ON CONTACT HEAT TRANSFER ON A SINGLE HEARTH FURNACE FLOOR USING DEM

N. HILSE[1], V. SCHERER[1]

[1] Institute of Energy Plant Technology (LEAT)
Ruhr-University Bochum (RUB)
Universitätsstraße 150, 44780 Bochum, Germany
e-mail: hilse@leat.rub.de, www.leat.ruhr-uni-bochum.de

Abstract. In the present paper, contact heat transfer on a batch-operated single circular floor of a multiple hearth furnace is numerically examined using the Discrete Element Method (DEM). The particles are agitated on the floor by a single rabble arm equipped with mixing blades. Two different rabble arm configurations are studied, a rabble arm with three blades covering just the area from the centre of the floor to the wall enclosing the circular floor, and a rabble arm with six blades, which covers the whole diameter of the floor. The floor temperature is set to 100°C, and the initial particle temperature is 20°C. Spherical particles made of aluminium and polyoxymethylene (POM) with two particle diameters (10 and 20 mm) are examined. Blade angle inclination is varied, namely, 0°, 45° and 90°. The major results are that for POM spheres the major mechanism dominating contact heat transfer is the gas layer in the vicinity of the contact point particle-floor, whereas for aluminium the heat transfer through the direct contact point of floor and particle is of equal importance as the heat transfer through the gas layer. For the first configuration with three blades, a larger blade angle leads to lower heat up rates, while the second configuration with six blades, increases the heating rate for larger blade angles.

Keywords: Granular Materials, DEM, Contact Heat Transfer.

1. INTRODUCTION

Multiple hearth furnaces are used in industry for the thermal treatment of solids. Typical examples are the calcination of minerals [1] such as magnesite, dolomite or kaolin but also the torrefaction of biomass [2]. The furnaces consist of multiple circular floors stacked above each other, on which the granular material is agitated by rotating rabble arms, typically one to four. These rabble arms are equipped with blades, which move the bulk material in radial direction, either to the periphery or the centre of the floor (see Figure 1). From there, the particles fall to the next subsequent floor. Radially installed burners are providing heat for the thermal treatment. The main heat transfer mechanisms are radiation and convection from the flame and contact heat transfer from the heated furnace floors.

The number of studies on multiple hearth furnaces is very small despite their industrial importance. As an example of some of the few works on this topic, the group of Wu et al. [4] presented a dynamic 1D process model for the calcination of kaolin in multiple hearth furnaces and used this model to derive control strategies for multiple hearth furnaces [5,6]. In addition,

Thomas et al. [7] determined the residence time of the solid material in a multi-opening kiln for kaolin production using talc as a tracer. In a recently presented study by Kriegeskorte et al. [8], particle mechanics on a single batch-operated furnace floor was examined.

The aim of the present work is to examine the influence of particle size, particle material, blade angle and the type of agitation on heat up of the bulk.

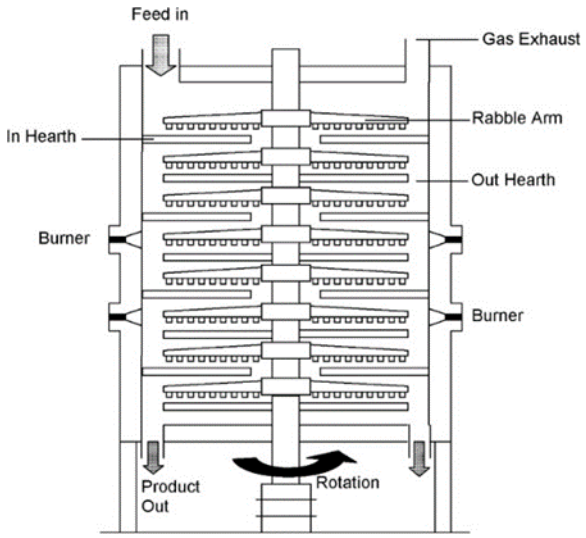

Figure 1: Schematic sketch of a multiple hearth furnace [1]

2. SET UP

In the current study, a model of a single hearth furnace floor operated in batch mode is used to evaluate contact heat transfer from the floor to the particle bulk. The configuration used for the DEM simulations is based on the design and dimensions of the test rig from [8]. The numerical model consists of a circular bottom plate with a diameter of 0.55 m. The central shaft has a diameter of 50 mm and carries the rabble arm which itself is equipped with blades with a total length of 60 mm and a thickness of 10 mm. The blade ends are half cylinders with an equivalent radius 10 mm. The blade inclination is adjustable.

Two versions of blade arms are used. The first version consists of three blades attached to the rabble arm (see Figure 2a). The blades are arranged in angles of either 90° (orthogonal to the rabble arm), 45° (as depicted in Figure 2a, transporting the bulk away from the centre) or 0° (parallel to the rabble arm). The second design is equipped with a doubled rabble arm (three additional blades on the opposite side of the central shaft), depicted in Figure 2b. The doubled rabble arm is designed in a way that one set of blades leads the bulk to the periphery of the floor (Figure 2b, left set) and the other set of blades redirects the bulk back to the centre of the floor. The first design is further on referred to as ’single-blade’ and the second configuration as ’double-blade’.

The particle bulk consists of spherical particles, which are heated by the heated floor, which is set to a constant temperature of 100°C. The initial particle temperature is 20°C. The number of simulated particles is determined according to their size so that a single layer of particles nearly completely covers the floor of the furnace (the calculated coverage of the floor is 82 %). Regarding 10 mm particles this corresponds to a number of 2424 particles with the single

bladed arm, in case of the 20 mm particles it is 606. In case of the double-bladed configuration, the particle number is slightly lower as the additional blades obstruct a further part of the floor area.

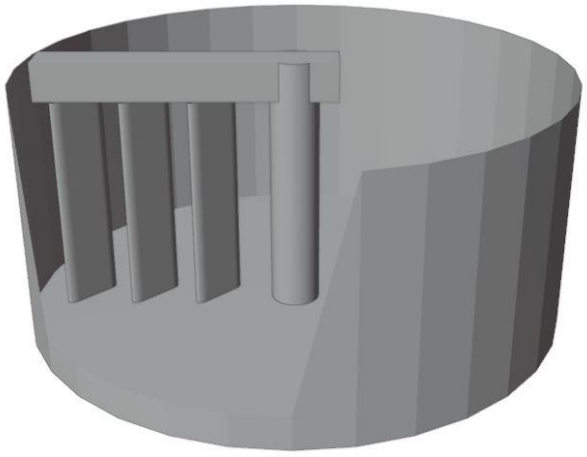

Figure 2a: 3D-Model of the hearth furnace floor – single-bladed rabble arm

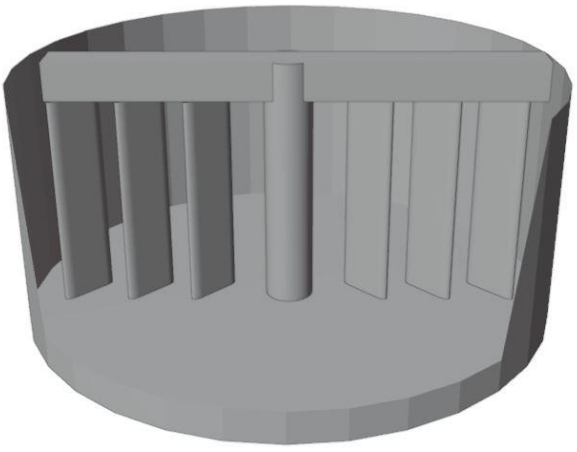

Figure 2b: 3D-Model of the hearth furnace floor – double-bladed rabble arm

3. DEM AND CONTACT HEAT TRANSFER MODEL

The DEM simulations were performed with an in house code. The equations for translational and rotational motion are given by the equations (1) and (2):

$$m_i \frac{d^2\vec{x}_i}{dt^2} = \sum_{j=1}^{N} \vec{F}_{ij} + m_i\,\vec{g}, \tag{1}$$

$$\theta_i \frac{d^2\vec{\varphi}_i}{dt^2} = \sum_{j=1}^{N} \vec{M}_{ij} = \sum_{j=1}^{N} \left(\vec{r}_i \times \vec{F}_{ij} + \vec{M}_j^r\right) \tag{2}$$

where m_i is the mass of the particle and its moment of inertia is θ_i. The linear acceleration is given by $d^2\vec{x}_i/dt^2$ and the angular acceleration of the particle is $d^2\vec{\varphi}_i/dt^2$. $\vec{F}_{ij}$ and $\vec{M}_{ij}$ are the external force and momentum induced by other particles or walls. $\vec{M}_j^r$ is the rolling friction torque. The distance from centre of gravity to the contact point of particle/particle or particle/wall is represented by $\vec{r}_i$. The equations are integrated numerically by an Euler-Cromer algorithm. To determine the contact forces, a linear spring-dashpot model is used. The parameters used for the simulations of the hearth furnace floor can be found in Table 1.

The basis of the contact heat transfer model used in the code is the model of Vargas and McCarthy [9,10]. The model consists of two parts, the direct heat transfer through the contact point of the two solids expressed by the contact conductivity H_g and the heat transferred through the stagnant gas layer in the vicinity of the contact expressed by the gas conductivity H_c. Both conductivities depend on the temperature difference between particle and floor. The total heat transferred reads as (eq. 3):

$$\dot{Q} = (H_c + H_g)\,\Delta T. \tag{3}$$

The contact conductivity can be calculated according to Hertz [11] by eq. (4) to (9). The contact radius a_c depends on the normal force $\vec{F}^n$ determined by the spring-damper model, the effective Young's modulus E_{eff}, the Poisson's ratio ϑ the effective radius r_{eff}. The thermal conductivity used is the harmonic mean λ_{harm} of the two materials:

$$H_C = 2\,\lambda_{harm} \cdot\ a_c. \tag{4}$$

$$a_c = \left(\frac{3 \cdot (1-\vartheta^2) \cdot \vec{F}^n \cdot r_{eff}}{2E_{eff}}\right)^{\frac{1}{3}} \tag{6}$$

$$E_{eff} = \frac{2E_iE_j}{E_i + E_j} \tag{7}$$

$$r_{eff} = \frac{2r_ir_j}{r_i + r_j} \tag{8}$$

$$\lambda_{eff} = \frac{2\lambda_i\lambda_j}{\lambda_i + \lambda_j} \tag{9}$$

The thermal conductivity H_g is then calculated from the reciprocal of the thermal resistance with the area exposed to the gas A_g, the thermal conductivity of the gas λ_g and the averaged length l_g over which the heat flux applies.

$$H_g = \frac{\lambda_g A_g}{l_g} \tag{10}$$

$$A_g = 2\pi r^2 \left[1 - \frac{1}{2}\left(\frac{a_c}{r}\right)^2\right] \tag{11}$$

$$l_g = \frac{r^2\left[1 - \frac{\pi}{4}\right]}{r - a_c} \tag{12}$$

The temperature change in the particles is resolved in a radial shell model, in which each shell has an individual but uniform temperature. Since the intra-particle heat transport is not simulated based on a 3D mesh, a directional temperature distribution is not resolved. All parameters used in for the DEM can be found in Table 1 and Table 2.

Table 1: DEM parameters spring-dashpot model

		POM Spheres			Aluminium Spheres		
		Sphere-Sphere	Sphere-Plate/Wall	Sphere-Blade/Shaft	Sphere-Sphere	Sphere-Plate/Wall	Sphere-Blade/Shaft
Coefficient of restitution	[-]	0.85	0.75	0.75	0.88	0.88	0.88

Collision time	[s]	6E-4	6E-4	6E-4	2E-4	2E-4	2E-4
Rolling friction	[-]	0.015	0.02	0.02	0.015	0.02	0.02
Sliding friction	[-]	0.3	0.3	0.25	0.3	0.3	0.25

Table 2: DEM parameters contact heat transfer

		POM	Aluminium	Steel	Air
Density	[kg/m³]	1420	2700	7700	-
Heat capacity	[J/(kgK)]	1460	900	466	-
Conductivity	[W/(mK)]	0.292	237	50	0.0262
Young's modulus	[Pa]	3.2e9	7.0e10	2e11	-
Poisson's ratio	[-]	0.44	0.33	0.27	-

4. RESULTS AND DISCUSSION

The simulations were performed for total times of 3000 to 6000 seconds, depending on particle size and material. To examine the influence of the different parameters, the heat transfer calculations were performed without any consideration of heat loss, except the heat, which is transferred to the steel parts of the test rig (the peripheral enclosure of the floor, the central shaft and the blades). Since the considered temperatures are sufficiently low, radiation effects can be neglected safely. Figure 3 shows the influence of the blade angle on the particle mechanics for the POM particles. The increasing of the blade angle results in an increasing heap formation in front of the blades, regarding a clockwise movement of the rabble arm. At the same time, the particle-free surface area of the furnace bottom plate increases behind the rabble arm. A detailed analysis of the particle mechanics can be found in [8]. An additional set of blades, the double-bladed configuration, decreases the particle-free surface area and the heap formation in front of the individual rabble arms. It increases the mixing of the particle bulk.

Figure 4 shows the temperature graphs of the single-bladed configuration for 20 mm spheres, which were agitated on the hot plate for 6000 s. The plots show the averaged surface temperature of all particles. The graphs on the left side represent the temperatures for POM spheres, while the graphs on the right side show the temperatures for aluminium spheres.

The changes in particle mechanics have a direct influence on the contact heat transfer. The blade angle causing the lowest mechanical impact on the particles (0°) shows the fastest heating rates. The increase of the blade angle results in an increased heap formation in front of the blades. This reduces the number of direct particle-bottom plate contacts, which leads to reduced heating rates. Also, the steady-state final temperature of the particle bed changes with blade angle for both materials, which is caused by the heat loss to the unheated parts of the hearth furnace. It increases the more spheres are in contact with the blades, the shaft and the surrounding walls, i.e. heat loss increases with increasing blade angle due to enhanced heap formation.

This also applies for the aluminium spheres, which, as expected, show faster heating rates in comparison to the POM spheres, and have about 10 K higher temperatures after 10 minutes simulated time (Figure 4, right).

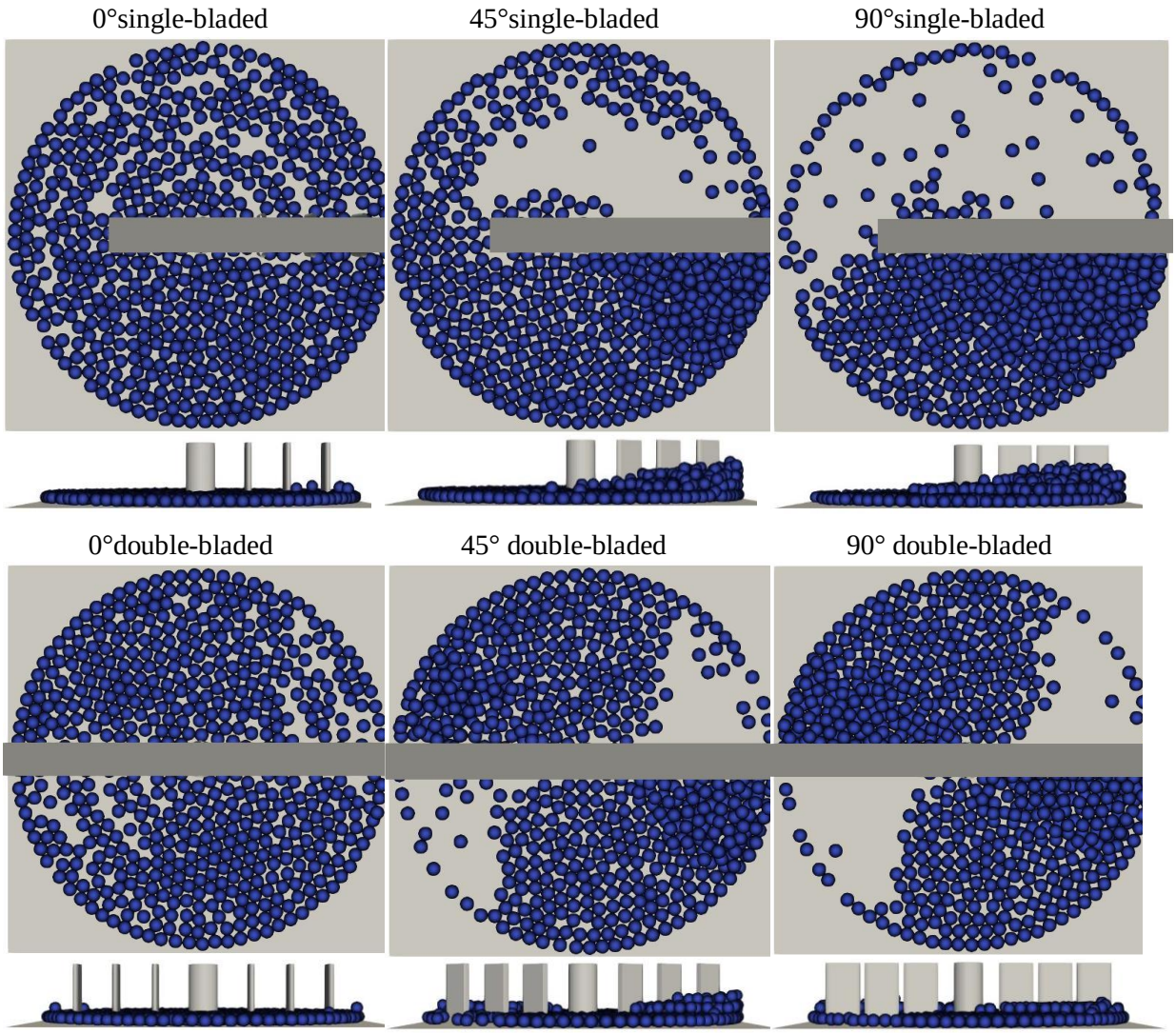

Figure 3: DEM Simulations of 20 mm POM spheres at different blade angles, top view and side view

The contribution of the two contact heat transfer phenomena (gas layer, direct solid contact) to the total contact heat transfer are very different for aluminium and POM. In the case of aluminium, the values for the contact conductivity H_c and conductivity through the gas layer H_g are approximately equal. For example, at a simulated time of 10 minutes H_c contributes 54.66 % and H_g contributes 45.34 % to the net conductivity. In contrast, the percentage of H_g is 99.51 % for POM spheres. This is mainly due to the low thermal conductivity of the POM (about 800 times smaller than for aluminium). This different contribution of the two contact heat transfer phenomena for POM and aluminium agrees with the finding of Fischer et al. [11]. In addition,

it shall be mentioned that the total heat flow acting on the POM spheres at 10 minutes simulated time corresponds to 64 % of the heat flow received by the aluminium spheres.

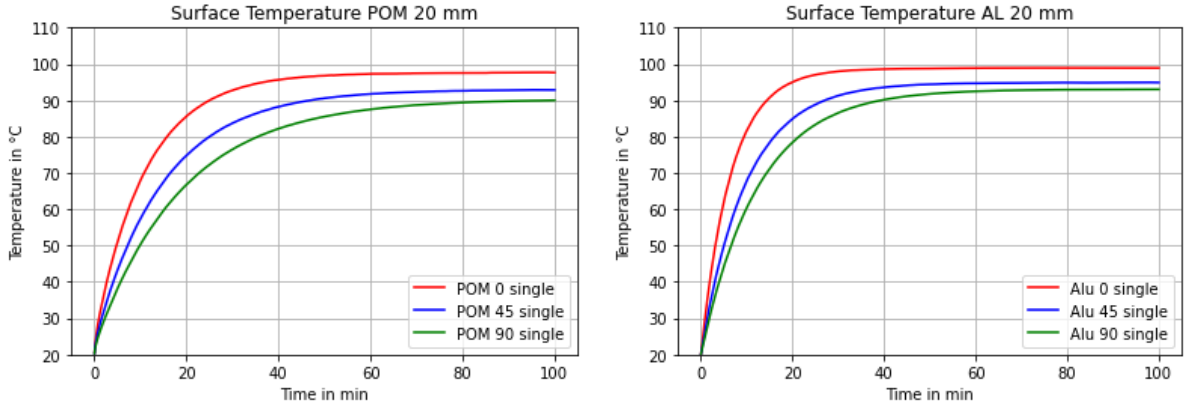

Figure 4: Surface Temperatures of POM (left) and aluminium (right) spheres of 20 mm diameter for different blade angles, single-bladed

An outstanding phenomena can be observed when evaluating the simulations with the double-bladed rabble arm (see Figure 5). By using a second set of blades, the number of spheres in contact with the heated plate at 90° blade angle is roughly doubled (compare Figure 3). This results in visibly higher heating rates for the double-bladed rabble arm than for the single-bladed rabble arm for both materials at 90°. However, this effect is not visible for the blade angles of 45 and 0°.

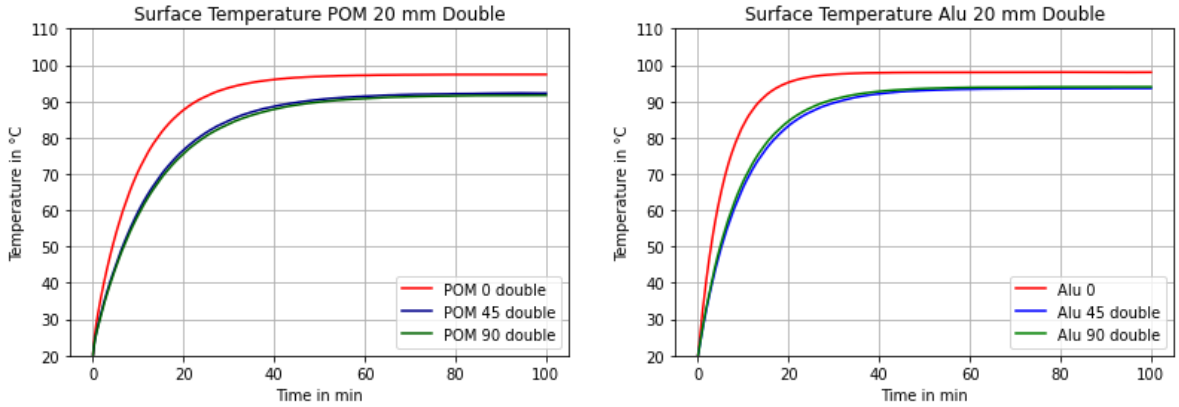

Figure 5: Surface Temperatures of POM (left) and aluminium (right) spheres of 20 mm diameter for different blade angles, Double-bladed

As expected, the 10 mm spheres heat up faster compared to the 20 mm spheres because of their reduced thermal capacity (see Figure 6). It is striking that the graphs for 10 mm POM spheres at 45° and 90° have a very similar progression in contrast to the 20 mm particles. The main reason for this is due to the changed geometry ratios of particles and blades. Due to their smaller diameter, the 10 mm spheres, unlike the 20 mm spheres, are hardly caught at the periphery when the blades are positioned at 45°.

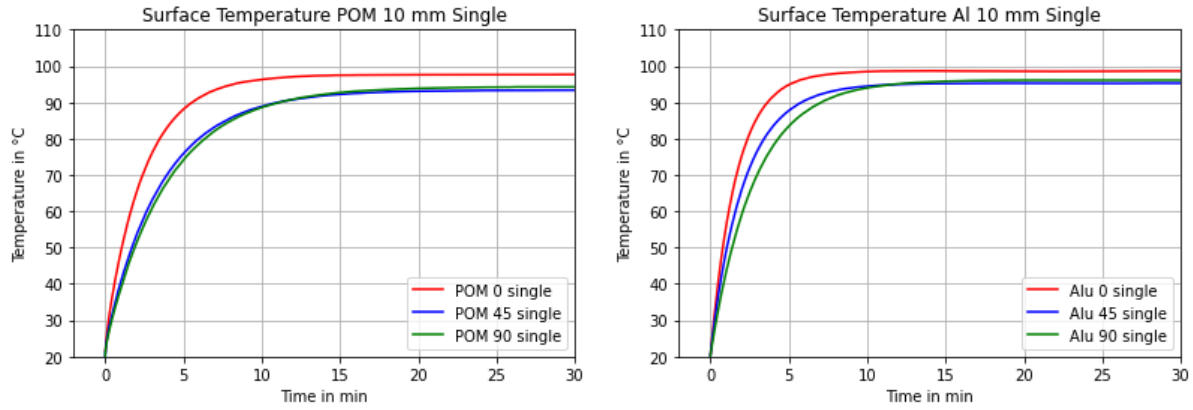

Figure 6: Surface Temperatures of POM (left) and aluminium (right) spheres of 10 mm diameter for different blade angles, single bladed

Evaluating the temperature distribution on the hearth furnace floor after 3000 s (see Figure 7) one can see that the 45° blade angle causes a significant higher number of particles with lower temperatures towards the non-heated outer walls of the furnace. For the 90° angle, mixing is effective over the entire radius of the bottom plate, but the piling up in front of the blades and the heat loss there leads to lower overall temperatures.

In case of the aluminium spheres, the mixing at 45° blade angle is marginally improved due to the difference in particle density. Due to this and an improved sphere-sphere heat transfer caused by the higher heat conductivity of aluminium the heating rates are slightly larger than at 90° blade angle. Over the total time, however, the final temperatures for both angles reach the same values because rather cold particles also accumulate at the outer edge of the bottom plate.

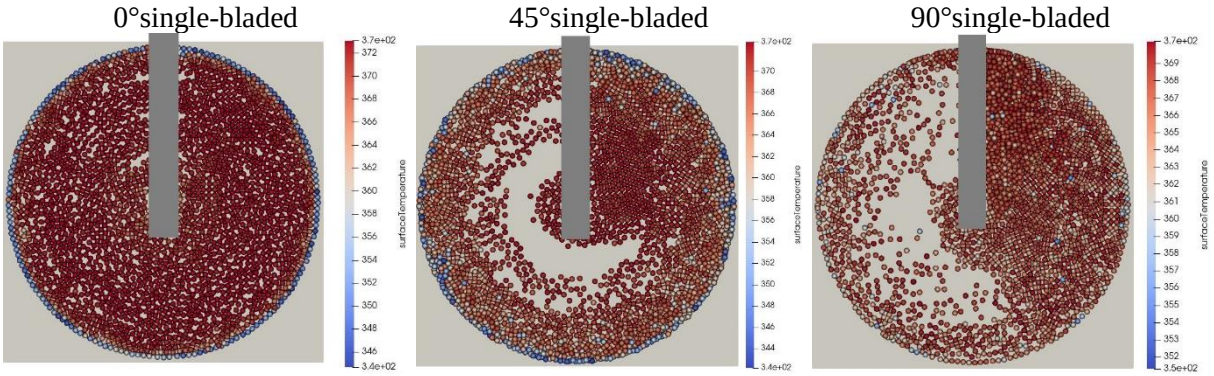

Figure 7: Temperature distribution on the hearth furnace after 3000 s simulation time for 10 mm POM spheres

Figure 8 shows the results of the 10 mm sphere simulations with the double-bladed rabble arm. In contrast to the 20 mm spheres, there are no larger heating rates present for the 90° blade angle. The increased heat flux due to the increased number of sphere-bottom plate contacts seems to be compensated by larger heat losses at the unheated parts of the hearth furnace. For the 45° blade angle, the extra set of blades works against the accumulation of particles next to the furnace walls, which leads in a more even temperature distribution and higher overall average temperatures compared to the single-bladed simulations.

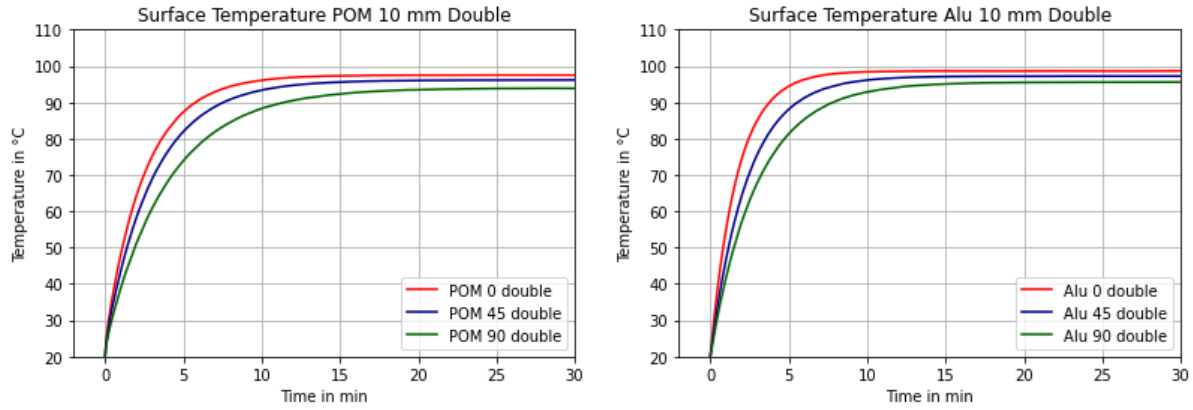

Figure 8: Surface Temperatures of POM (left) and aluminium (right) spheres of 10 mm diameter for different blade angles, double bladed

5. CONCLUSIONS

Contact heat transfer is examined of initially cold spherical polyoxymethylene (POM) and aluminium particles, which are in contact with a heated circular floor. The particles are agitated by a rotating shaft equipped with mixing blades. The results show that for all cases the angular blade position with the lowest mechanical influence on particle bulk mechanics shows the fastest heating rates. This is due to the fact that an increasing blade angle increases accumulation of the spheres in front of the rabble arm, which reduces the number of contacts of spheres and heated bottom plate. At the same time, the number of contacts with the unheated parts of the furnace increases, which leads to larger heat losses and hence to lower terminal temperatures in steady state. Due to the higher thermal conductivity, the heating rates of the aluminium spheres are, as expected, larger.

In case of POM spheres, the simulations show that contact heat transfer is mainly determined by heat transfer is the gas layer in the vicinity of the contact point particle-floor (~99%). The larger thermal conductivity of aluminium leads to equal importance of heat transfer through contact of solids and through the gas layer in the vicinity of the contact point.

The 10 mm particles show that here, the degree of mixing has a higher influence on the average temperature. For the intermediate angular position of 45 degrees, there is a clearly recognizable accumulation of particles at the edge of the base plate where spheres with significantly lower temperatures concentrate. Spheres with higher temperatures are located more towards the middle of the bottom plate.

It can be summarised that for the larger particles considered here (POM and aluminium, 20 mm diameter), an increase in the heating rates can be observed for the highest blade angle (90°) when an additional set of blades is used (2x3 blades on opposite sides instead of 1x3 blades on only one side of the shaft). This is due to an increased number of sphere-bottom plate contacts. For the 10 mm spheres, this effect is seen at 45° blade angle and is due to an improved mixing of the bulk. At 0° blade angle, however, the larger number of contacts with the heated surface is compensated by an equally larger number of contacts with unheated surfaces, which cool the spheres.

Acknowledgement: This work has been funded by the Deutsche Forschungsgemeinschaft (DFG, German Research Foundation) – 422037413–CRC/TRR 287 "BULK-REACTION".
Diese Arbeit wurde gefördert und finanziert durch die Deutsche Forschungsgemeinschaft (DFG) – 422037413–CRC/TRR 287 "BULK-REACTION".

REFERENCES

[1] A. Eskelinen, A. Zakharov, S.-L. Jämsä-Jounela, und J. Hearle, „Dynamic modeling of a multiple hearth furnace for kaolin calcination“, *AIChE J.*, Bd. 61, Nr. 11, S. 3683–3698, Nov. 2015, doi: 10.1002/aic.14903.

[2] K. Lampe, G. Grund, R. Erpelding, und J. Denker, „Biocoal preparation - Biomass a sustainable fuel for industrial processes“, *Proceedings - European Metallurgical Conference, EMC 2011*, Bd. 5, S. 1623–1630, Jan. 2011.

[3] X. Liu und J. Jiang, „Mass and Heat Transfer in a Continuous Plate Dryer“, *Drying Technology*, Bd. 22, Nr. 7, S. 1621–1635, Dez. 2004, doi: 10.1081/DRT-200025619.

[4] Y.-L. Wu, Z.-Y. Jiang, X.-X. Zhang, Q.-G. Xue, A.-B. Yu, und Y.-S. Shen, „Modeling of Thermochemical Behavior in an Industrial-Scale Rotary Hearth Furnace for Metallurgical Dust Recycling“, *Metall Mater Trans B*, Bd. 48, Nr. 5, S. 2403–2418, Okt. 2017, doi: 10.1007/s11663-017-1034-5.

[5] F. J. V. Gomez und S. L. Jämsä-Jounela, „Control Strategy For A Multiple Hearth Furnace“, *IFAC-PapersOnLine*, Bd. 51, Nr. 21, S. 189–194, 2018, doi: 10.1016/j.ifacol.2018.09.416.

[6] S.-L. Jämsä-Jounela, J. V. Gomez Fuentes, J. Hearle, D. Moseley, und A. Smirnov, „Control strategy for a multiple hearth furnace in kaolin production“, *Control Engineering Practice*, Bd. 81, S. 18–27, Dez. 2018, doi: 10.1016/j.conengprac.2018.08.020.

[7] R. Thomas, D. Grose, G. Obaje, R. Taylor, N. Rowson, und S. Blackburn, „Residence time investigation of a multiple hearth kiln using mineral tracers“, *Chemical Engineering and Processing: Process Intensification*, Bd. 48, Nr. 4, S. 950–954, Apr. 2009, doi: 10.1016/j.cep.2009.01.003.

[8] M. Kriegeskorte, N. Hilse, P. Spatz, und V. Scherer, „Experimental study on influence of blade angle and particle size on particle mechanics on a batch-operated single floor of a multiple hearth furnace“, *Particuology*, Bd. 85, S. 224–240, Feb. 2023, doi: 10.1016/j.partic.2023.06.009.

[9] W. L. Vargas und J. J. McCarthy, „Heat conduction in granular materials“, *AIChE J.*, Bd. 47, Nr. 5, S. 1052–1059, Mai 2001, doi: 10.1002/aic.690470511.

[10] W. L. Vargas und J. J. McCarthy, „Conductivity of granular media with stagnant interstitial fluids via thermal particle dynamics simulation“, *International Journal of Heat and Mass Transfer*, Bd. 45, Nr. 24, S. 4847–4856, Nov. 2002, doi: 10.1016/S0017-9310(02)00175-8.

[11] J. Fischer *u. a.*, „Particle-particle contact heat transfer models in thermal DEM: A model comparison and experimental validation“, *Powder Technology*, Bd. 429, S. 118909, Nov. 2023, doi: 10.1016/j.powtec.2023.118909.